energies

MDPI

Article

Efficiency of Recycling Double-Pass V-Corrugated Solar Air Collectors

Chii-Dong Ho *, Ching-Fang Hsiao, Hsuan Chang, Yi-En Tien and Zih-Syuan Hong

Energy and Opto-Electronic Materials Research Center, Department of Chemical and Materials Engineering, Tamkang University, Tamsui, New Taipei 251, Taiwan; tvxqdbskshw8938@gmail.com (C.-F.H.); nhchang@mail.tku.edu.tw (H.C.); tienyien@gmail.com (Y.-E.T.); aux1212tw@yahoo.com.tw (Z.-S.H.)

* Correspondence: cdho@mail.tku.edu.tw; Tel.: +886-2-26215656 (ext. 2724); Fax: +886-2-26209887

Received: 31 May 2017; Accepted: 26 June 2017; Published: 29 June 2017

Abstract: The influence of recycling on double-pass solar air collectors with welding of the V-corrugated absorber has been studied experimentally and theoretically. Welding the V-corrugated absorber and the recycle-effect concept to the solar air collector was proposed to strengthen the convective heat-transfer coefficient due to turbulence promotion. Both the recycle effect and the V-corrugated absorber can effectively enhance the heat transfer efficiency compared to various designs such as single-pass, flat-plate double-pass, and double-pass wire mesh packed devices. Recycling operations and welding the V-corrugated absorber could enhance the collector efficiency by increasing the recycle ratio, incident solar radiations, and air mass flow rates. The most efficient and economical operating conditions were found at $R \approx 0.5$, with relatively small hydraulic dissipated energy compensation. It was found that the turbulence intensity increase from welding the V-corrugated absorber into the solar air collector channel could compensate for the power consumption increase, when considering economic feasibility.

Keywords: solar air heater; V-corrugated absorber; recycle effect; heat-transfer efficiency; double-pass operation

1. Introduction

New designs of solar air collectors with welding of the V-corrugated absorber into double-pass devices under recycling operations has been proposed and studied, as shown in Figure 1a,b. The experimental setup was fabricated with the V-shape corrugated absorber welded on the flat-plate solar air collector to validate the theoretical predictions calculated by mathematical modeling. A higher device performance was obtained with a recycling double-pass V-corrugated collector than with a flat-plate solar air collector of the same working dimensions. El-Sebaii and Shalaby [1] and Sevik [2] discussed the design and experimental investigation of solar dryers. Razika, et al. [3] and Al-Kayiem, Yassen [4] studied the inclination angel for the absorption–convection heat transfer behavior in a solar air collector. El-Sebaii and Al-Snani [5] investigated the effects of various selective coating materials on the collector's performance. Improvement of solar collector efficiency in many devices has been investigated by introducing free convection [6] and force convection [7], extending heat transfer area [8], and increasing flow turbulence in a solar air heater channel with vortex generators [9,10] and welding V-ribs [11]. The application of the recycle effect concept to solar air heaters has been confirmed with technical feasibility in double-pass [12] and multi-pass [13] operations, and the recycling double-pass design with eddy promotion [14,15] results in enhancement of the convective heat-transfer coefficient. The new designs in the present study of solar air collectors were investigated, adopting the V-corrugated recycling double-pass device to increase the convective heat-transfer coefficients due to both the enhancement of flow turbulence and enlargement of the heat-transfer area, as shown in Figure 1a,b, respectively.

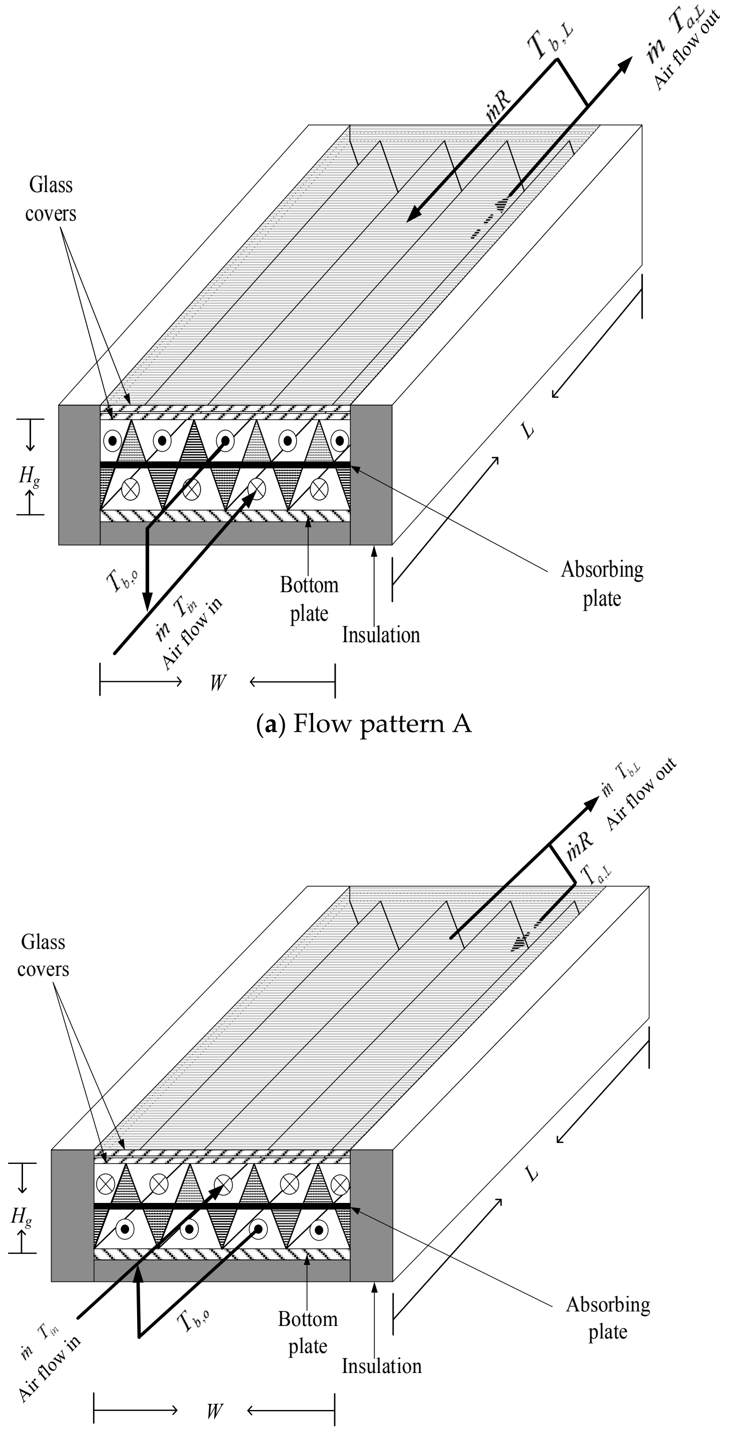

(**a**) Flow pattern A

(**b**) Flow pattern B

Figure 1. Configuration of recycling double-pass V-corrugated solar air collectors.

The purposes of the present study are: (a) to carry out theoretical predictions and experimental runs of operating the recycling double-pass V-corrugated solar air collector; (b) to investigate the influences of the recycle ratio and air mass flow rate on the heat-transfer efficiency enhancement and power consumption; (c) to investigate the economic feasibility of the new design of the recycling double-pass V-corrugated solar air collectors.

2. Theoretical Analysis

Consider the heat transfer in two subchannels with welding of the V-corrugated absorber plate to divide a parallel conduit of height H_g, length L and width W, as shown in Figure 1a,b with the different air flow arrangements. Before entering the lower subchannel (flow pattern A), as shown in Figure 1a, the inlet air mass flow rate $\dot{m}$ and inlet temperature T_{in} is premixed with the recycling air flow $R\dot{m}$ exiting from the upper subchannel with the outlet temperature $T_{a,L}$. The inlet air mass may flow through the upper channel firstly (flow pattern B), as shown in Figure 1b.

By following the same mathematical treatment and experimental methods performed in our previous work [16], except welding the V-corrugated absorber instead of packing wire mesh, the theoretical solutions of the temperature distributions of the flowing air in the lower and upper subchannels were obtained, making the energy balance on a finite system element, as shown in Figure 2. The various heat transfer coefficients at different components of the solar air heater were sketched in the thermal resistance network in Figure 3. The results are:

$$T_a(\xi) = C_1 e^{Y_1 \xi} + C_2 e^{Y_2 \xi} - \frac{B_3 B_4 - B_1 B_6}{B_2 B_4 - B_1 B_5} + T_s \tag{1}$$

$$T_b(\xi) = \frac{Y_1 - B_5}{B_4} C_1 e^{Y_1 \xi} + \frac{Y_2 - B_5}{B_4} C_2 e^{Y_2 \xi} + \frac{B_3 B_5 - B_2 B_6}{B_2 B_4 - B_1 B_5} + T_s \tag{2}$$

The definitions of B_i, G_i, M_i, Y_i, C_i, F_i, and I_i are referred to in the Appendix A. In obtaining the above results for the steady-state one-dimensional mathematical formulation, the boundary conditions are:

$$z = 0,\ T_a(0) = T_{a,0} = \frac{T_{in} + RT_b(0)}{1 + R} \tag{3}$$

$$z = L,\ T_a(1) = T_{a,L},\ T_b(1) = T_{b,L} \tag{4}$$

The outlet temperature of $T_{a,L}$ can be calculated from Equation (1).

$$T_a(1) = C_1 e^{Y_1} + C_2 e^{Y_2} - \frac{B_3 B_4 - B_1 B_6}{B_2 B_4 - B_1 B_5} + T_s \tag{5}$$

The useful energy gained by the flowing air was estimated from the energy balance on the lower subchannel, upper subchannel, and whole solar air collector with the known inlet and outlet temperatures, respectively.

$$Q_u = \dot{m}(1+R)C_p(T_{a,L} - T_{a,0}) + \dot{m}C_p(T_{b,0} - T_{b,L}) = \dot{m}C_p(T_{a,L} - T_{a,i}) \tag{6}$$

The collector efficiency η_V of the recycling double-pass V-corrugated solar air collector was obtained from the actual useful energy gained by the airflow and the incident solar radiation as:

$$\begin{aligned} \eta_V &= \frac{Q_u(\text{Useful gain of energy carried away by air})}{I_0 A_c(\text{Total solar radiation incident})} \\ &= \frac{\dot{m}C_p\left(T_{a,L} - T_{a,i}\right)}{I_0 A_c} = \frac{I_0 \tau_g^2 \alpha_p - U_L(T_{p,m} - T_s)}{I_0} \end{aligned} \tag{7}$$

The average absorber temperature was readily obtained, equating the terms of Equation (7) as:

$$T_{p,m} = T_s + (I_0 \tau_g^2 \alpha_p / U_L) - \frac{\dot{m}C_p(T_{a,L} - T_{a,i})}{A_c U_L} \tag{8a}$$

$$= T_s + (I_0/U_L)\left(\tau_g^2 \alpha_p - \eta_V\right) \tag{8b}$$

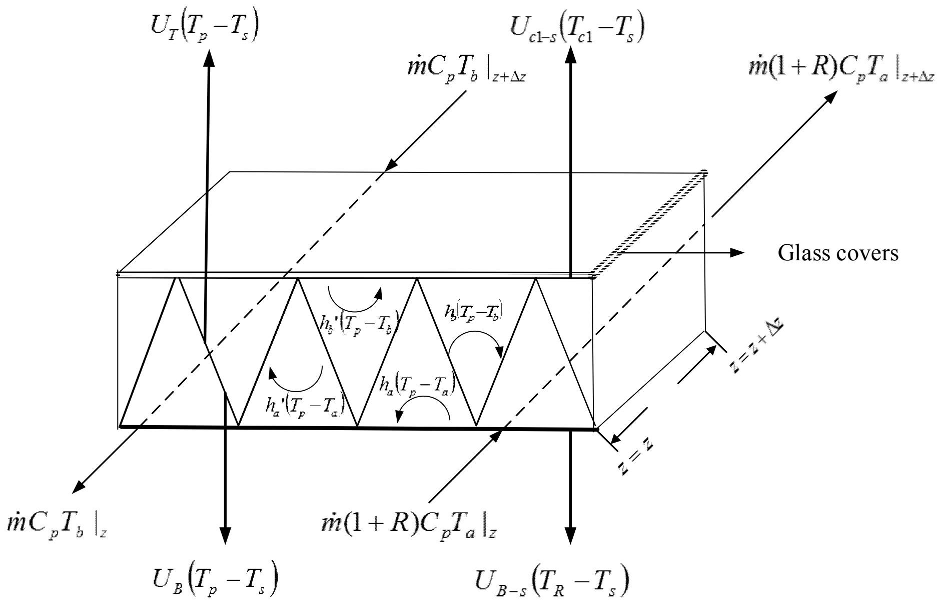

Figure 2. The energy balance in a finite system element (flow pattern A).

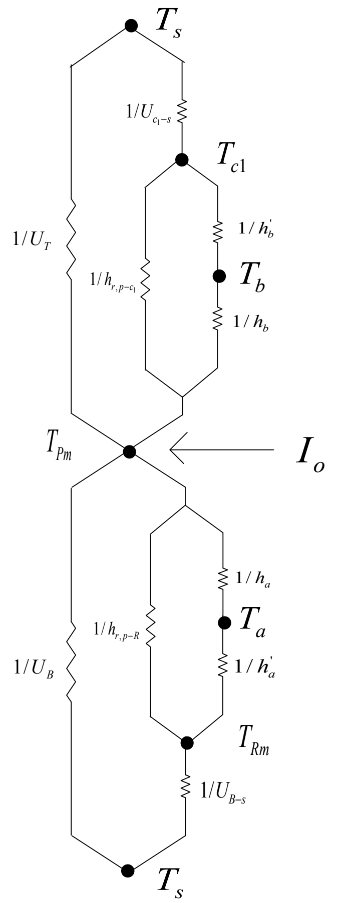

Figure 3. Schematic diagram of V-corrugated solar air heaters as a thermal network.

3. Experimental Setup

The recycling double-pass solar air collectors are welded to four units of V-shape stainless steel absorbing plate of 7×10^{-5} m thickness on the bottom plate to divide the air flow conduit of width

W, length L, and height H_g into two subchannels, as shown in Figure 4 (flow pattern A). A photo of the experimental device was taken and shown in Figure 5. Three configurations of solar air collectors, such as the downward single-pass device, recycling double-pass wire mesh, and recycling double-pass V-corrugated absorber were investigated theoretically and experimentally. The experimental runs were conducted using a blower (Teco 3 Phase Induction Motor, Model BL model 552, Redmond Co, Owosso, MI, USA) to supply the ambient air, and the air mass flow rate was measured using an anemometer (Kanmax Japan Inc., Osaka, Japan). The device parameters [17] and operating conditions are as follows: $L = W = 0.3$ m; $H_g = 0.062$ m; $k_s = 46.64$ W/m·K; $\tau_g = 0.875$; $\alpha_p = 0.95$; $\varepsilon_g = 0.94$; $\varepsilon_p = 0.8$; $\varepsilon_R = 0.94$; $I_0 = 830$ and 1100 W/m^2; $T_{in} = 293$,303 and 313 K; $V = 1.0$ m/s; $\dot{m} = 0.0107$, 0.0161 and 0.0214 kg/s; $T_s = 293$ K, $\sigma = 5.68 \times 10^{-8}$ W/m^2·K^4. The calculation methods for flow pattern B are similar to those in the previous section of flow pattern A. A comparison of both flow patterns in Figure 6 indicates a greater collector performance improvement in operating flow pattern A is higher than that in the flow pattern B. Therefore, all the theoretical predictions and experimental works were carried out using flow pattern A as an illustration in the present study. The evaluation procedure for collector efficiency is now described. With known device geometries (W, L, H_g), physical properties (k_s, τ_g, α_p, ε_g, ε_p, ε_R, C_p, μ, ρ) and the given operating conditions (I_0, T_{in}, V, $\dot{m}$, T_s), a temporary η_V is first estimated from Equation (7) using Equation (8a) for calculating $T_{a,L}$ once $T_{p,m}$ is assumed. The $T_{p,m}$ value is thus re-checked using Equation (8b) by continued iterations, and the final value η_V was obtained until the last value meets the required convergence. The theoretical predictions were obtained by substituting the specified values of physical properties and operation conditions into the appropriate equations, and the results are represented in Figures 7 and 8 for comparison. The influence of the recycle ratio on collector efficiencies of theoretical predictions and experimental results for various incident solar radiations, recycle ratios, and air mass flow rates are presented in Figures 7 and 8, respectively.

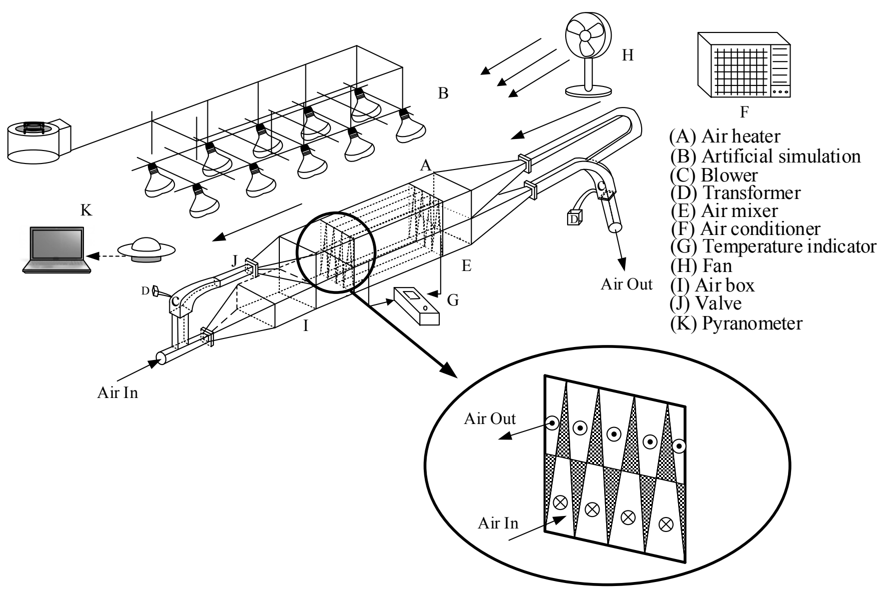

Figure 4. Schematic of a recycling double-pass V-corrugated solar air heater (flow pattern A).

Figure 5. A photo of the experimental device.

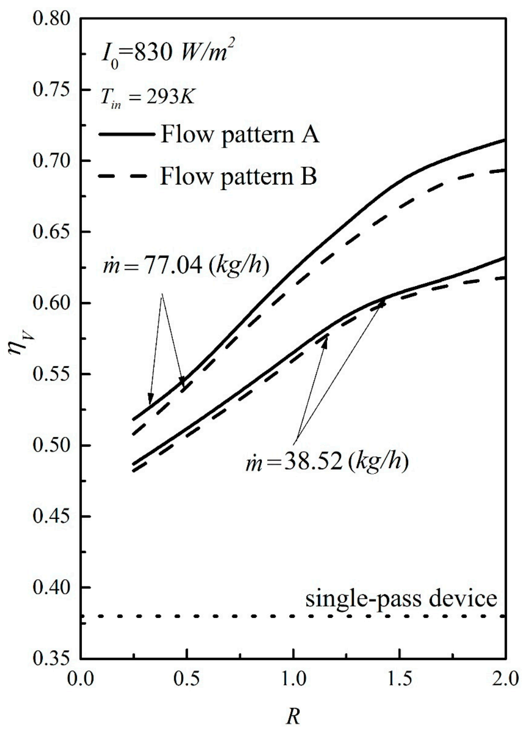

Figure 6. Collector efficiencies of both flow patterns (I_0 = 830 W/m^2).

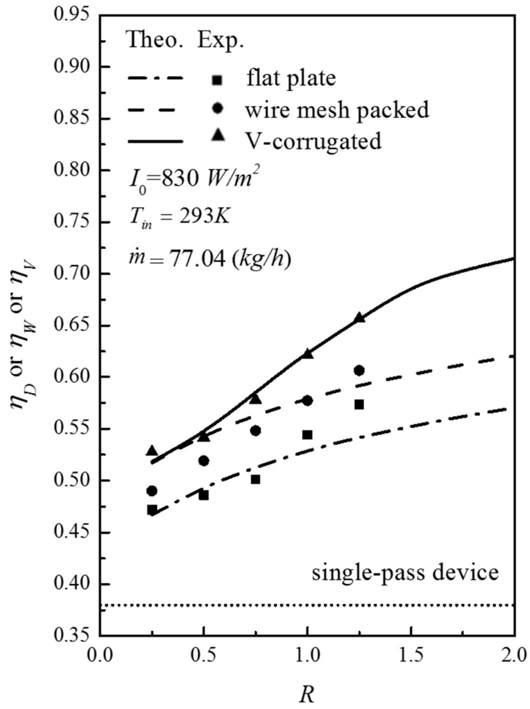

Figure 7. Effect of recycle ratio on collector efficiency (I_0 = 830 W/m^2).

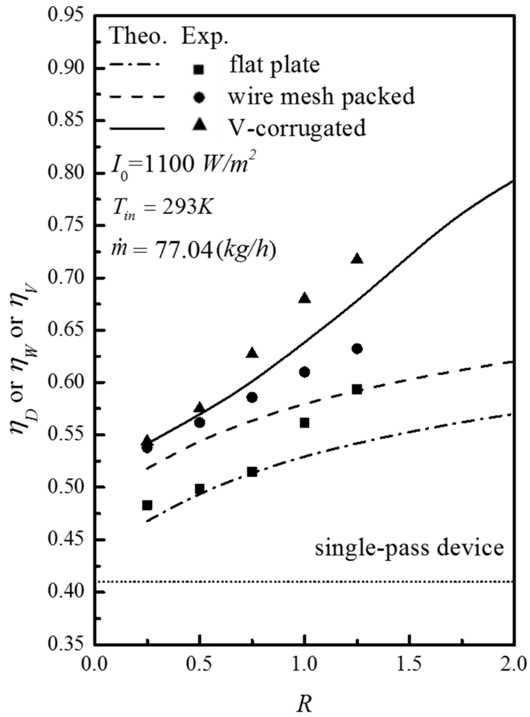

Figure 8. Effect of recycle ratio on collector efficiency (I_0 = 1100 W/m^2).

Moffat [18] determined the experimental uncertainty of each individual measurement directly from the experimental run as follows:

$$S_{\eta_{exp}} = \left\{ \sum_{i=1}^{N_{exp}} \frac{\left(\eta_{exp,i} - \overline{\eta}_{exp,i}\right)^2}{N-1} \right\}^{1/2} \tag{9}$$

and the mean value of the resulting experimental uncertainty was defined by:

$$S_{\overline{\eta}_{\exp}} = \frac{S_{\eta_{\exp}}}{\sqrt{N_{\exp}}} \tag{10}$$

Estimations of the experimental uncertainty for I_0 = 830 and I_0 = 1100 W/m^2 with three air mass flow rates were calculated. The mean experimental uncertainty of the measurements in Figures 7 and 8 ranged between $2.60 \times 10^{-3} \le S_{\overline{\eta}_{\exp}} \le 7.46 \times 10^{-3}$. Meanwhile, the difference of the experimental results from the theoretical predictions may be defined as:

$$E = \frac{1}{N_{\exp}} \sum_{i=1}^{N_{\exp}} \frac{\left|\eta_{theo,i} - \eta_{\exp,i}\right|}{\eta_{theo,i}} \times 100\% \tag{11}$$

Difference deviations between the theoretical and experimental values were quantified and calculated using Equation (11) within $0.13 \le E \le 2.85$ under two solar radiation incidents for two configurations without (flat-plate type) and with attaching wire mesh. A fairly good agreement between theoretical predictions and experimental runs was achieved.

4. Collector Efficiency Improvement

By following the same mathematical treatment and experimental methods performed in our previous work [16], except welding the V-corrugated absorber instead of packing with wire mesh, the device performance improvements of the three types of recycling double-pass devices, namely flat-plate, wire mesh, and V-corrugated devices, were defined as the improvement of each collector's efficiency, I_D, I_W and I_V , as defined by Equations (12)–(14), respectively, relative to that of the downward-type single-pass device of the same working dimensions, as follows:

$$I_D = \frac{\text{collector efficiency of flat} - \text{plate double} - \text{pass device}, \ \eta_D}{\text{collector efficiency of downward } \sin\text{gle} - \text{pass device}, \ \eta_S} - 1 \tag{12}$$

$$I_W = \frac{\text{collector efficiency of wire mesh double} - \text{pass device}, \ \eta_W}{\text{collector efficiency of downward } \sin\text{gle} - \text{pass device}, \ \eta_S} - 1 \tag{13}$$

$$I_V = \frac{\text{collector efficiency of double} - \text{pass V} - \text{corrugated}, \ \eta_V}{\text{collector efficiency of downward } \sin\text{gle} - \text{pass device}, \ \eta_S} - 1 \tag{14}$$

in which η_D, η_W, η_S and η_V denote collector efficiencies of the double-pass flat-plate device, multi-pass flat-plate device, the baffled device with fins attached, the downward-type single-pass device, and the V-corrugated device, respectively. The present work is actually the extension of previous work [16], except with welding of the V-corrugated absorber. The collector efficiencies of η_D, η_W and η_S were investigated in our previous work [16] and the collector efficiency improvements of I_D, I_W and I_V for the devices of the flat-plate, wire mesh, and V-corrugated absorbers were calculated in Equations (12)–(14), respectively, for comparison.

5. Results and Discussion

The calculation methods and procedures were performed exactly the same as those of our previous work [16], and thus, the results will be discussed. All the theoretical predictions and experimental results of η_D, η_W and η_V increase with the recycle ratio and incident solar radiations, as seen from Figures 7 and 8.

It is indicated from Figures 7 and 8 that the collector efficiency of the V-corrugated solar air collector is higher than those of the flat-plate and wire mesh devices. The collector efficiency increase with recycle ratio and air mass flow rate, especially for the V-corrugated device when operating at the higher recycle ratio, as confirmed by Table 1. Restated, the collector efficiency η_V increases with increasing recycle ratios and air mass flow rates due to a higher convective heat-transfer coefficient being achieved. Furthermore, Figure 9 gives a graphical representation of the collector performance improvements of I_D, I_W, and I_V for the flat-plate, wire mesh packed, and V-corrugated double-pass devices under the same operating conditions, respectively. The collector performance improvement decreases with the air mass flow rate to a more remarkable extent, while the improvement increases with the recycle ratio, as shown in Figure 9 and Table 1 as well. However, the collector efficiency improvement of the V-corrugated solar air collector is better than other recycling configurations such as flat-plate and wire mesh packed solar air collectors for all mass flow rates and recycle ratios. Moreover, the hydraulic dissipated energy and power consumption increases owing to recycling double-pass operation with the V-corrugated absorber are defined as:

$$P_V = \dot{m}(1+R)\ell w_{f,a} + \dot{m}\ell w_{f,b} = \dot{m}(1+R)\frac{2f_{F,a}\overline{v}^2 L}{D_{e,a}} + \dot{m}\frac{2f_{F,b}\overline{v}^2 L}{D_{e,b}}, \quad (15)$$

double-pass V-corrugated device.

$$f_{F,i} = f + y\frac{W}{L}, \quad (16)$$

for V-corrugated device [19], i = a, b.

$$f = \frac{24}{Re}, y = 0.9, \text{ for } Re < 2550 \quad (17)$$

$$f = 0.0094, y = 2.92\ Re^{-0.15}, \text{ for } 2550 < Re < 10^4 \quad (18)$$

$$f = 0.059Re^{-0.2}, y = 0.73, \text{ for } 10^4 < Re < 10^5 \quad (19)$$

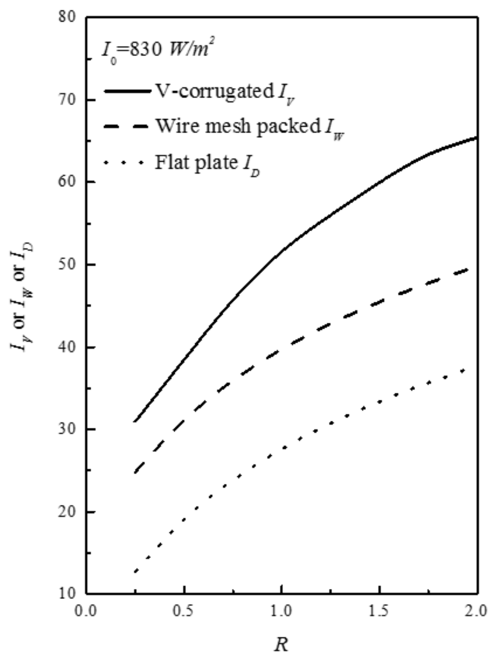

Figure 9. Comparisons of collector efficiency between the present device and the previous work [16].

Table 1. Theoretical predictions of heat-transfer efficiency improvements in a V-corrugated device of η_V and I_V for I_0 = 830 W/m^2 and I_0 = 1100 W/m^2.

Mass Flow Rate	Recycle Ratio	I_0 = 830 (W/m^2)		I_0 = 1100 (W/m^2)	
m (kg/h)	R	η_V	$I_V(\%)$	η_V	$I_V(\%)$
38.52	0.25	0.487	57.60	0.510	69.51
	0.5	0.511	65.52	0.535	77.85
	0.75	0.538	73.99	0.563	86.88
	1	0.565	82.89	0.592	96.58
	1.25	0.593	91.86	0.623	106.87
	1.5	0.608	96.79	0.655	117.45
	1.75	0.618	99.97	0.685	127.48
	2	0.632	104.58	0.704	134.01
57.96	0.25	0.503	35.98	0.530	45.62
	0.5	0.526	42.07	0.553	52.01
	0.75	0.565	52.76	0.578	58.86
	1	0.597	61.34	0.622	70.99
	1.25	0.630	70.32	0.658	80.84
	1.5	0.663	79.15	0.697	91.55
	1.75	0.676	82.65	0.744	104.32
	2	0.688	85.97	0.766	110.40
77.04	0.25	0.508	21.94	0.508	29.34
	0.5	0.536	28.46	0.536	36.06
	0.75	0.580	39.11	0.580	43.41
	1	0.614	47.29	0.614	55.44
	1.25	0.651	56.04	0.651	64.83
	1.5	0.688	65.03	0.688	75.58
	1.75	0.703	68.68	0.703	85.69
	2	0.715	71.41	0.715	92.99

The power consumption increase for the double-pass V-corrugated devices $I_{P,V}$ is defined relative to that in the downward single-pass operation $P_S = \dot{m}\ell w_{f,s} = \frac{2 f_{F,S} \bar{v}^2 L}{D_{e,S}}$ as:

$$I_{P,V} = \frac{P_V - P_S}{P_S}, \tag{20}$$

the V-corrugated device.

Similarly, for the flat-plate device and wire mesh packed device:

$$I_{P,D} = \frac{P_D - P_S}{P_S}, \tag{21}$$

the flat-plate device.

$$I_{P,W} = \frac{P_W - P_S}{P_S}, \tag{22}$$

the wire mesh packed device.

The effects of various recycle ratios and air mass flow rates on the ratio of both the efficiency improvement and the power consumption, $I_D/I_{P,D}$, $I_W/I_{P,W}$ and $I_V/I_{P,V}$ for various configurations were calculated and presented for comparison and for making an economic judgement to demonstrate feasible operating conditions. The higher value of $I_V/I_{P,V}$ is obtained in operating recycling double-pass V-corrugated solar air collectors, as demonstrated in Figure 10. The extent of collector efficiency improvement is more notable with recycle ratio for the recycling double-pass V-corrugated solar air collectors than for the flat-plate and wire mesh packed devices. With this comparison, the advantage of the present design is evident.

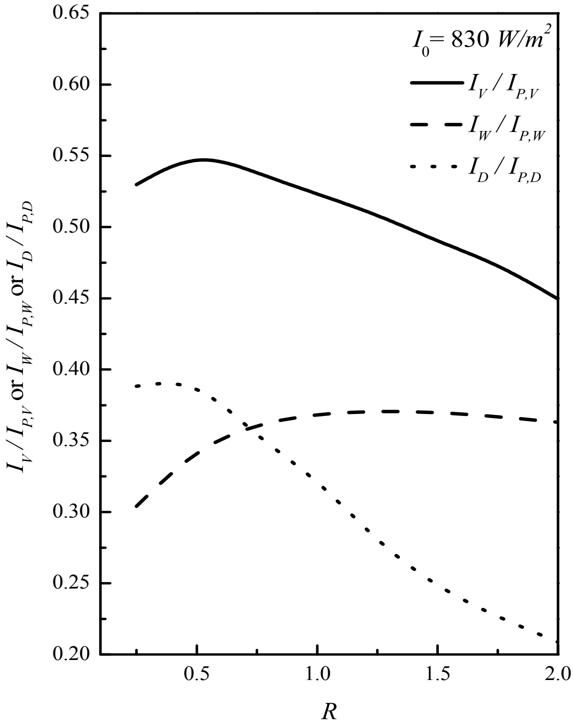

Figure 10. The ratio of I_V / I_P vs. recycle ratio R for various configurations.

6. Conclusions

The strategies for improving the performance of recycling double-pass V-corrugated solar air collectors are either the preheating effect or enhancing the convective heat-transfer coefficient. The improvement of collector efficiency in such devices with welding of the V-corrugated absorber has been investigated analytically and experimentally. The introduction of external recycling creates a positive effect on the heat transfer, which provides better collector efficiency due to the enhanced convective heat-transfer coefficient. This is caused by an increase in the turbulence of air flowing above and under the V-corrugated absorber. The improvement in device performance is obtainable by using a recycling double-pass V-corrugated device rather than without recycling or by using flat-plate devices, as indicated in Figures 7 and 8. Moreover, the ratio of I_V / I_P , alongside recycle ratio and air mass flow rate, were represented in Figure 10 to investigate the optimal operation conditions for considering the economic feasibility of various double-pass configurations. The present findings can be summarized as follows: (1) Application of the recycling double-pass V-corrugated solar air collector is technically and economically feasible as compared to both of the flat-plate and wire mesh packed solar air collectors; (2) Collector performance increases with increasing the recycle ratio but with decreasing the air mass flow rate, and with the inlet air flowing through the lower channel first (flow pattern A), device performance is higher than that in the device with the inlet air flowing through the upper channel first (flow pattern B); (3) The optimal recycle ratio for both economic and technical operation, with relatively small compensation for increased hydraulic dissipated energy, was found to be $R \approx 0.5$; (4) The advantage of the present device is evident, and the present study provides an important contribution to solar air collectors by coupling external recycling and different geometric designs of absorbing plates.

Acknowledgments: The authors wish to thank the Ministry of Science and Technology of the Republic of China for the financial support.

Author Contributions: This paper is a result of the full collaboration of all the authors. However, the concept for this research was conceived by Chii-Dong Ho, Ching-Fang Hsiao contributed to mathematical derivations, Hsuan Chang and Zih-Syuan Hong elaborated the manuscript preparation, and Yi-En Tien performed the experiments.

Conflicts of Interest: The authors declare no conflict of interest.

Nomenclature

A_c	Surface area of the collector = LW (m^2)
B_i	Coefficients defined in Equations (A1)–(A6)
C_i	Coefficients defined in Equations (A16) and (A17)
C_p	Specific heat of air at constant pressure (J/(kg K))
$D_{e,0}$	Equivalent diameter of downward-type single-pass device (m)
$D_{e,a}$	Equivalent diameter of lower subchannel of double-pass device (m)
$D_{e,b}$	Equivalent diameter of upper subchannel of double-pass device (m)
E	Deviation of the experimental measurements from theoretical predictions, defined in Equation (11)
F_i	Coefficients defined in Equations (A18)–(A20)
f_F	Fanning friction factor
G_i	Coefficients defined in Equations (A7)–(A13)
H_g	Height of channels (m)
h_a	Convection coefficient between the absorber plate and subchannel a (W/(m^2 K))
h_b	Convection coefficient between the absorber plate and subchannel b (W/(m^2 K))
$h_{r,p-c1}$	Radiation heat transfer coefficient between cover 1 and absorber plate (W/m^2 K)
$h_{r,p-R}$	Radiation heat transfer coefficient between absorber plate and bottom plate (W/m^2 K)
h_w	Convective heat transfer coefficient for air flowing over the outside surface of glass cover (W/(m^2 K))
I_0	Incident solar radiation (W/m^2)
I_D	Percentage of collector efficiency improvement, defined in Equation (12)
I_P	Power consumption increment, defined in Equations (20)–(22)
I_W	Percentage of collector efficiency improvement, defined in Equation (13)
I_V	Percentage of collector efficiency improvement, defined in Equation (14)
k_s	Thermal conductivity of insulator (W/(m K))
L	Channel length (m)
l_s	Thickness of insulator (m)
$\ell w_{f,a}$	Lower subchannel friction loss of double-pass device (J/kg)
$\ell w_{f,b}$	Upper subchannel friction loss of double-pass device (J/kg)
$\ell w_{f,s}$	Friction loss of downward-type single-pass device (J/kg)
$\dot{m}$	Total air mass flow rate (kg/h)
N	Number of glass cover
N_{exp}	Number of experimental measurements
Nu	Nusselt number
P_D	Power consumption of the flat plate double-pass device (W)
P_S	Power consumption of downward-type single-pass device (W)
P_V	Power consumption of the V corrugated double-pass device (W)
P_W	Power consumption of the wire mesh packed double-pass device (W)
Q_u	Useful energy gained by air (W)
R	Recycle ratio, reverse air mass flow rate divided by input air mass flow rate
$S_{\eta_{\text{exp}}}$	The experimental uncertainty of an individual measurement
$S_{\overline{\eta}_{\text{exp}}}$	The mean value of $S_{\eta_{\text{exp}}}$
Re	Reynolds number
$T_{a,i}$	Inlet air temperature (K)
$T_{a,0}$	The mixing temperature of the subchannel a at $x = 0$ (K)
$T_{a,L}$	The temperature of the subchannel a at $x = L$ (K)
$T_{b,0}$	The temperature of the subchannel b at $x = 0$ (K)
$T_{b,L}$	The temperature of the subchannel b at $x = L$ (K)
$T_a(z)$	Axial fluid temperature distribution in subchannel a (K)
$T_b(z)$	Axial fluid temperature distribution in subchannel b (K)
T_{c1}	Temperature of glass cover 1 (K)

T_p	Temperature of absorbing plate (K)
$T_{p,m}$	Mean temperature of absorbing plate (K)
T_s	Ambient temperature (K)
U_B	Loss coefficient from the bottom of solar air heater to the ambient environment (W/(m^2 K))
U_{B-s}	Loss coefficient from the surfaces of edges and the bottom of the solar collector to the ambient environment (W/m^2 K)
U_{c1-s}	Loss coefficient from the inner cover to the ambient environment (W/m^2 K)
U_T	Loss coefficient from the top of solar air heater to the ambient environment (W/m^2 K)
W	Width of both upper and lower subchannels (m)
$\overline{v_s}$	Mean air velocity in the downward-type single-pass device (m/s)
$\overline{v_a}$	Mean air velocity in subchannel *a* of double-pass device (m/s)
$\overline{v_b}$	Mean air velocity in subchannel *b* of double-pass device (m/s)
Y_i	Coefficients defined in Equations (A14) and (A15)
z	Axial coordinate (m)
Greek Letters	
α_p	Absorptivity of the absorbing plate
η_D	Collector efficiency of the flat-plate double-pass device
η_S	Collector efficiency of the downward type single-pass device
η_V	Collector efficiency of the double-pass V-corrugated solar air ter
η_W	Collector efficiency of the double-pass wire mesh packed solar air heater
$\eta_{\exp,i}$	Experimental data of collector efficiency
$\overline{\eta}_{\exp,i}$	The mean value of the experimental data $\eta_{\exp,i}$
$\eta_{theo,i}$	Theoretical prediction of collector efficiency
μ	Air viscosity (kg/ms)
τ_g	Transmittance of glass cover
ε_g	Emissivity of glass cover
ε_p	Emissivity of absorbing plate
ρ	Air density (kg/m^3)
ξ	Dimensionless channel length

Appendix A

$$B_1 = -WL\left(h_b G_1 + h_b h_{r,p-c_1} G_1 G_4 - U_{c_1-s} h_b G_4\right)/R\dot{m}C_p \tag{A1}$$

$$B_2 = -WL\left(h_b G_2 + h_b h_{r,p-c_1} G_2 G_4\right)/R\dot{m}C_p \tag{A2}$$

$$B_3 = -WL\left(h_b G_3 + h_b h_{r,p-c_1} G_3 G_4\right)/R\dot{m}C_p \tag{A3}$$

$$B_4 = WL\left(h_a G_6 + h_a h_{r,p-R} G_6 G_7\right)/(1+R)\dot{m}C_p \tag{A4}$$

$$B_5 = WL\left(h_a G_5 + h_a h_{r,p-R} G_5 G_7 - U_{B-s} h_a G_7\right)/(1+R)\dot{m}C_p \tag{A5}$$

$$B_6 = WL\left(h_a G_3 + h_a h_{r,p-R} G_3 G_7\right)/(1+R)\dot{m}C_p \tag{A6}$$

$$G_1 = -(h_a + U_T + U_B)/(U_T + U_B + h_a + h_b) \tag{A7}$$

$$G_2 = h_a/(U_T + U_B + h_a + h_b) \tag{A8}$$

$$G_3 = I_0 a_p \tau_g^2/(U_T + U_B + h_a + h_b) \tag{A9}$$

$$G_4 = \left(h_{r,p-c_1} + h_b + U_{c_1-s}\right)^{-1} \tag{A10}$$

$$G_5 = -(h_b + U_T + U_B)/(U_T + U_B + h_a + h_b) \tag{A11}$$

$$G_6 = h_b/(U_T + U_B + h_a + h_b) \tag{A12}$$

$$G_7 = \left(h_{r,p-R} + h_a + U_{B-s}\right)^{-1} \tag{A13}$$

$$Y_1 = \frac{(B_1 + B_5) + \sqrt{(B_1 - B_5)^2 + 4B_2B_4}}{2} \tag{A14}$$

$$Y_2 = \frac{(B_1 + B_5) - \sqrt{(B_1 - B_5)^2 + 4B_2B_4}}{2} \tag{A15}$$

$$C_1 = \frac{1}{F_1}\left[\frac{F_2 I_2 e^{Y_2} - B_4(F_2 - F_3)(1 + R - \mathrm{Re}^{Y_2})}{I_2 e^{Y_2}(1 + R - \mathrm{Re}^{Y_1}) - I_1 e^{Y_1}(1 + R - \mathrm{Re}^{Y_2})}\right] \tag{A16}$$

$$C_2 = -\frac{1}{F_1}\left[\frac{F_2 I_1 e^{Y_1} - B_4(F_2 - F_3)(1 + R - \mathrm{Re}^{Y_1})}{I_2 e^{Y_2}(1 + R - \mathrm{Re}^{Y_1}) - I_1 e^{Y_1}(1 + R - \mathrm{Re}^{Y_2})}\right] \tag{A17}$$

$$F_1 = B_1B_5 - B_2B_4 \tag{A18}$$

$$F_2 = B_3B_4 - B_1B_6 \tag{A19}$$

$$F_3 = B_2B_6 - B_3B_5 \tag{A20}$$

$$I_1 = Y_1 - B_4 - B_5 \tag{A21}$$

$$I_2 = Y_2 - B_4 - B_5 \tag{A22}$$

References

1. El-Sebaii, A.A.; Shalaby, S.M. Experimental investigation of an indirect-mode forced convection solar dryer for drying thymus and mint. *Energy Convers. Manag.* **2013**, *74*, 109–116. [CrossRef]
2. Sevik, S. Design, experimental investigation and analysis of a solar drying system. *Energy Convers. Manag.* **2013**, *8*, 27–34.
3. Razika, I.; Nabila, I.; Madani, B.; Zohra, H.F. The effects of volumetric flow rate and inclination angle on the performance of a solar thermal collector. *Energy Convers. Manag.* **2014**, *78*, 931–937. [CrossRef]
4. Al-Kayiem, H.H.; Yassen, T.A. On the natural convection heat transfer in a rectangular passage solar air heater. *Sol. Energy* **2015**, *12*, 10–18. [CrossRef]
5. El-Sebaii, A.A.; Al-Snani, H. Effect of selective coating on thermal performance of flat plate solar air heaters. *Energy* **2010**, *35*, 1820–1828. [CrossRef]
6. Vaziri, R.; Ilkan, M.; Egelioglu, F. Experimental performance of performance of perforated glazed solar air heaters and unglazed transpired solar air heater. *Sol. Energy* **2015**, *119*, 251–260. [CrossRef]
7. Sharma, K.S.; kalamkar, V.R. Experimental and numerical investigation of forced convection heat transfer in solar air heater with thin ribs. *Sol. Energy* **2017**, *147*, 227–291. [CrossRef]
8. Fudholi, A.; Sopian, K.; Othman, M.Y.; Ruslan, M.H.; Bakhtyar, B. Energy analysis and improvement potential of finned double-pass solar collector. *Energy Convers. Manag.* **2013**, *75*, 234–240. [CrossRef]
9. Tamna, S.; Skullong, S.; Thianpong, C.; Promvonge, P. Heat transfer behaviors in a solar air heater channel with multiple V-baffle vortex generators. *Sol. Energy* **2014**, *110*, 720–735. [CrossRef]
10. Skullong, S.; Promvonge, P.; Thianpong, C.; Pimsarn, M. Thermal performance in solar air heater channel with combined wavy-groove and perforated-delta wing vortex generators. *Sol. Appl. Therm. Eng.* **2016**, *100*, 611–620. [CrossRef]
11. Maithani, R.; Saini, J.S. Heat transfer and friction factor correlations for a solar air heater duct roughened artificially with V-ribs with symmetrical gaps. *Exp. Therm. Fluid Sci.* **2016**, *70*, 220–227. [CrossRef]
12. El-Sebaii, A.A.; Aboul-Enein, S.; Ramadan, M.R.I.; Shalaby, S.M.; Moharram, B.M. Investigation of thermal performance of double-pass flat and v-corrugated plate solar air heaters. *Energy* **2011**, *36*, 1076–1086. [CrossRef]
13. Garg, H.P.; Sharma, V.K.; Bhargava, A.K. Theory of multiple-pass solar air heaters. *Energy* **1985**, *10*, 589–599. [CrossRef]
14. Wijeysundera, N.E.; Ah, L.L.; Tjioe, L.E. Thermal performance study of two-pass solar air heaters. *Sol. Energy* **1982**, *28*, 363–370. [CrossRef]
15. Singh, S.; Dhiman, P. Thermal and thermohydraulic performance evaluation of a novel type double pass packed bed solar air heater under external recycle using an analytical and RSM (response surface methodology) combined approach. *Energy* **2014**, *72*, 344–359. [CrossRef]
16. Ho, C.D.; Lin, C.S.; Chuang, Y.C.; Chao, C.C. Performance improvement of wire mesh packed double-pass solar air heaters with external recycle. *Renew. Energy* **2013**, *57*, 479–489. [CrossRef]

17. Gupta, M.K.; Kaushik, S.C. Performance evaluation of solar air heater for various artificial roughness geometries based on energy, effective and energy efficiencies. *Renew. Energy* **2009**, *34*, 465–476. [CrossRef]
18. Moffat, R.J. Describing the uncertainties in experimental results. *Exp. Therm. Fluid Sci.* **1988**, *1*, 3–17. [CrossRef]
19. Verma, R.; Chandra, R.; Garg, H.P. Optimization of solar air heaters of different designs. *Renew. Energy* **1992**, *2*, 521–531. [CrossRef]

© 2017 by the authors. Licensee MDPI, Basel, Switzerland. This article is an open access article distributed under the terms and conditions of the Creative Commons Attribution (CC BY) license (http://creativecommons.org/licenses/by/4.0/).